Research in Astronomy and Astrophysics, 22:115016 (14pp), 2022 November https://doi.org/10.1088/1674-4527/ac9577

An Ultra-wide Bandwidth Low-frequency Radio Astronomical Cryogenic Receiver for FAST Telescope

Hong-Fei Liu[1,2,3], Peng Jiang[1,2], Chuan He[4], Fan Yang[5], Hong-Ju Liu[6], Sheng-Wang Wang[4], Yang Wu[5], Yan Zhu[1,2], Yang Cao[1,2], Jin-You Song[1,2], Xiang-Wei Shi[1,2], Ming-Lei Guo[1,2], Hang Zhang[1,2], and Wen-Hao Liu[1,3]
[1] National Astronomical Observatories, Chinese Academy of Sciences (CAS), Beijing 100101, China; lhf@bao.ac.cn, pjiang@bao.ac.cn
[2] CAS Key Laboratory of FAST, National Astronomical Observatories, Chinese Academy of Sciences, Beijing 100101, China
[3] School of Astronomy and Space Science, University of Chinese Academy of Sciences, Beijing 101408, China
[4] The 16th Research Institute of China Electronic Technology Group Corporation, Hefei 230043, China
[5] The 54th Research Institute of China Electronics Technology Group Corporation, Shijiazhuang 050081, China
[6] Beijing Technology and Business University, Beijing 100048, China
Received 2022 July 2; revised 2022 August 27; accepted 2022 September 26; published 2022 November 2

Abstract

This paper presents an ultra-wide bandwidth (UWB) low-frequency radio astronomical cryogenic receiver for the Five-hundred-meter Aperture Spherical radio Telescope (FAST). It covers 6.6:1 bandwidth from 0.5 to 3.3 GHz. The receiver consists of a Quad-Ridged Flared Horn (QRFH), a cryogenic microwave unit, an optical transceiver and a warm microwave and frequency mixing unit. A QRFH with a concentric-loaded dielectric spear is developed: the average return losses are larger than 20 dB; the average ports polarization isolation is 43.87 dB; the average dish efficiency is higher than 65%. Many UWB cryogenic low loss components are developed for the fabrication of a cryogenic microwave unit. The average noise temperature lower than 14.2 K and 22.5 K are achieved as referred to the input ports of cryogenic Dewar and the output of horn, respectively. Compared to other similar advanced UWB receivers, such as Parkes 0.7–4.2 GHz (6:1 bandwidth) receiver and FAST 0.27–1.62 GHz (6:1 bandwidth) receiver, wider relative bandwidth of the proposed receiver is achieved and it is a new attempt to expand the bandwidth of UWB low-frequency receiver.

Key words: telescopes – methods: analytical – methods: observational

1. Introduction

The Five-hundred-meter Aperture Spherical radio Telescope (FAST) is designed to operate in the band of 0.07–3 GHz (Nan 2006). By 2019, six single pixel receivers with octave bandwidth have been developed to provide the coverage across the working band of FAST. In addition, a 19-beam receiver with a bandwidth of 1.05–1.45 GHz has also been fabricated for high efficiency sky survey (Jiang et al. 2020), at the expense of a relatively narrow bandwidth. One of the six single pixel receivers is an ultra-wide bandwidth (UWB) low-frequency receiver covering the band of 0.27–1.62 GHz (Smith & Weinreb 2016), which is mainly used for FAST commissioning and early science observation. The first discovery realized by FAST (Qian et al. 2019) is based on the application of this receiver, which benefits from the technological developments in UWB components, especially in Quad-Ridged Flared Horn (QRFH) (Akgiray et al. 2013), Silicon–Germanium (GeSi) wideband cryogenic low noise amplifier (LNA) (Weinreb et al. 2007).

More than ten years ago, a number of log-periodic type UWB feeds with dual linear polarization were developed due to increasing interest in multi-octave radio astronomy. The main four of them are Sinuous Feed (4:1 in bandwidth), Eleven Feed (7:1), ATA Feed (10:1) and QSC Feed (10:1) (Yang et al. 2011). Although they can realize UWB (near-constant beamwidth and phase center), two obvious disadvantages arising from the intrinsic features of log-periodic type limit their application on various telescopes. Their beamwidths are tough to be changed to adapt the reflector antennas with various ratio of focal length to aperture. In addition, their coaxial ports are differential inputs with 200–270 Ω nominal impedance (Yang et al. 2011) and require at least two differential LNAs (Eleven Feed requires four) to achieve gain and phase matching for one polarization. The resulting problem is that it is difficult to obtain UWB cryogenic differential LNA, and the noise temperature of the existing lowest noise UWB cryogenic differential LNA is still more than twice that of the single ended LNA (Bardin & Weinreb 2010). On the other hand, ridged horn or waveguide is another way to realize multi-octave bandwidth. The fundamental theory is that the ridges lower the dominant mode cutoff frequency by about four times in dual-ridged waveguides, compared with hollow waveguides (Hopfer 1955). Further, the single-mode relative bandwidth, that is, the cutoff wavelength ratio of dominant mode to next higher order mode, is largely expanded. Dual-ridged waveguide or horn can only obtain single linear polarization, so

further studies based on finite element method and magnetic field integral equations on quad-ridged structures to support dual linear polarizations are arising. As a result, QRFH achieves near-constant 10 dB nominal beamwidth over 5:1 bandwidth. At the time, the beamwidth of QRFH (the subtended angle to the reflector) is feasible to adjust in the range of 30°–140° due to the flared structure (Sun & Balanis 1994). This means that QRFH is suitable for different optical configurations. Another advantage in application of QRFH is that its input nominal impedance could be fabricated in the range of 50–100 Ω and requires only one single-ended LNA for each polarization. The above two flexibilities facilitate the application of UWB low-frequency receiver equipped with QRFH to radio astronomy telescopes, two of which the pioneers are 0.27–1.62 GHz UWB cryogenic receiver on FAST (Smith & Weinreb 2016) and 0.7–4.2 GHz UWB fully cryogenic receiver on Parkes (Hobbs et al. 2020). The bandwidth of the above two receivers is 6:1. The former covers a lower frequency, and its feed works at room temperature; the latter has higher frequency and its feed works at cryogenic temperature.

In order to improve the capability of simultaneous multi-spectrum line observation of FAST, this paper develops a 0.5–3.3 GHz UWB receiver with a concentric-loaded dielectric spear QRFH. The main differences or improvements of this proposed receiver with the first UWB cryogenic receiver for FAST are as follows: benefiting from the application and optimization of loading dielectric and overall optimal design of QRFH, the proposed receiver feed achieves wider relative and absolute bandwidths; one UWB optical transceiver delivers the full bandwidth signals of one polarization from the cryogenic unit to the warm unit via 3 km optical fibers with good gain flatness and resultantly improves the coherence in phase and amplitude of sub-band signals; wider absolute bandwidth requires more complicated filtering and frequency mixing networks. Focusing on improving antennas aperture efficiency, deep optimization to geometry parameters of horn and central dielectric spear extends the bandwidth of QRFH to 6.6:1. A dual-layer dielectric spear helps to further expand the beamwidth at the high-frequency band. A low-loss coaxial air line through one ridge with center conductor connected to the opposite ridge is used to form a balun at the base of the horn to excite one polarization. Therefore, only two single-ended LNAs are required for this horn, and the average return loss is larger than 20 dB for each coaxial input port.

The proposed QRFH has to work in the atmosphere (300 K) due to its large size determined by the low-end frequency coverage as low as 0.5 GHz. A helium cooling system based on Gifford-McMahon (GM) cycle (Thirumaleshwar & Subramanyam 1986) is fabricated to cool frontend low-noise microwave components of receiver and resultantly reduce receiver noise level, such as directional couplers, LNAs and power splitter. This cooling system consists of a vacuum Dewar, helium cryogenerator and compressor. A rectangular Dewar structure with a removable side plate is adopted for the purpose of quick replacement the internal microwave components. Reasonable hermeticity design and precision thermal analysis are implemented. The vacuum degree of 10^{-5} Pa, the first stage cryocooler temperature of 13 K and the second stage cryocooler temperature of 42 K are achieved inside the assembled Dewar. The directional coupler is used to inject calibrating noise signals to two polarization channels of receiver, and optimal design to microstrip structure directional coupler achieves good component performance at 15 K physical temperature: the coupling coefficient is larger than 25 dB, the insertion loss is smaller than 0.2 dB and the return losses are larger than 20 dB. Low Noise Factory, Inc. (LNF) and Cosmic Microwave Technology, Inc. (CMT) developed the best performing commercial UWB cryogenic LNAs: LNC0.3-14A (LNC0.3-14A datasheet 2022) from LNF and CITLF3 (CITLF3 datasheet 2022) from CMT. The former covers wider bandwidth from 0.3 to 14 GHz and claims 4.2 K noise temperature, while, the return loss is not large enough for this application bandwidth. CITLF3 with lower than 5 K noise and larger than 10 dB return loss from 0.01 to 4 GHz is resultantly employed for the proposed receiver. Low-noise optimal design for the cryogenic microwave unit achieves good noise characteristic across UWB: the average noise temperature lower than 14.2 K and 22.5 K are achieved as referred to the input ports of cryogenic Dewar and the output of horn, respectively.

Following the cryogenic microwave links, UWB warm optics and microwave electronics are fabricated, mainly including UWB optical transceiver, splitters and filters network and frequency transformer unit. Compared with other high-performance UWB low-frequency astronomical receivers worldwide (shown in Table 1), the proposed receiver extends the bandwidth to 6.6:1 and achieves appropriately low noise at the same time.

2. Design and Fabrication of Receiver

The block diagram and physical image of the proposed UWB receiver are shown in Figures 1 and 2, respectively. The receiver mainly consists of QRFH, cryogenic microwave unit, noise calibrating unit, optical transceiver, splitters and filters network, and warm microwave and frequency mixing unit. Based on state-of-the-art technologies, all front-end components from the feed to the optical transceiver are designed as full bandwidth components of 0.5–3.3 GHz. While, in view of the limitation of sampling bandwidth of digital backend, the frequency mixing unit is designed to have four sub-channels: 0.5–1, 0.9–1.8, 1.7–2.6 and 2.5–3.3 GHz. The two adjacent sub channels have 0.1 GHz frequency bands overlapping each other to ensure the data integrity of UWB observation. Based on the noise theory for a cascaded system described in Equation (1),

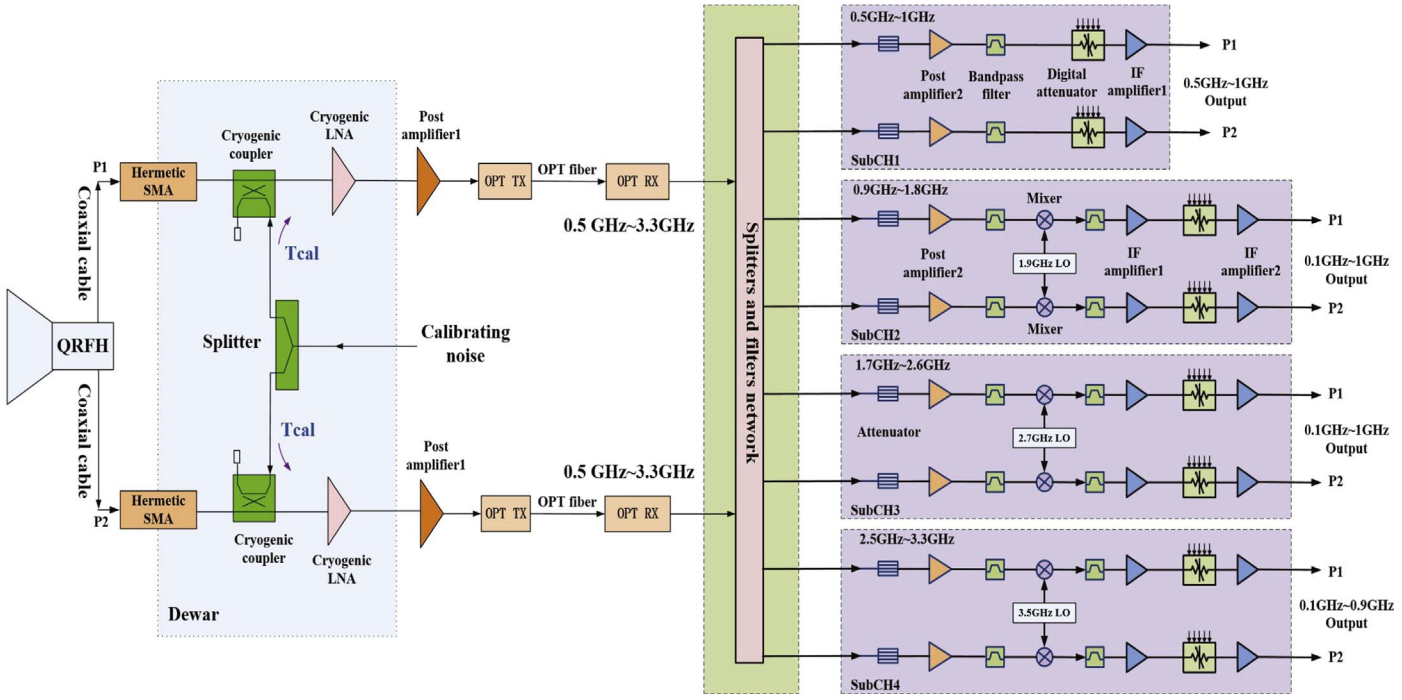

Figure 1. Block diagram of FAST 0.5–3.3 GHz UWB low-frequency cryogenic receiver. QRFH, cryogenic Dewar, UWB cryogenic microwave components, UWB optical transceiver, splitters and filters network, and warm microwave and frequency mixing unit are shown.

Table 1
Comparison of Main Performances of Similar Receivers Worldwide

Development Institutions	Operating Frequencies	Relative Bandwidth	Noise Temperatures
CALTECH (Smith & Weinreb 2016)	0.27–1.62 GHz	6:1	23 K (referred to feed output)
CSIRO (Hobbs et al. 2020)	0.7–4.2 GHz	6:1	9 K (referred to feed aperture)
This paper	0.5–3.3 GHz	**6.6**:**1**	22.5 K (referred to feed output)

the noise contribution of microwave parts in front of first stage LNA in microwave chain must be as low as possible to achieve overall low noise performance.

$$T_e = T_{e1} + \frac{T_{e2}}{G_1} + \frac{T_{e3}}{G_1 G_2} + \ldots \quad (1)$$

Applied to receiver chain, T_e is the equivalent noise temperature of receiver system; T_{e1} is contributed by QRFH, warm coaxial cable, hermetic connector, insulation cables and cryogenic directional coupler; T_{e2} is the noise temperature of cryogenic LNA; T_{e3} are noise temperature of backstage components of cryogenic LNA. And G_1 and G_2 are power gain of front-end passive components and cryogenic LNA. Because the feed of the proposed receiver is working in room temperature, the ohmic loss of passive components in front of cryogenic LNA must be optimized as much as possible.

System design analysis on physics temperature ($T_{\rm amb}$), average gain in logarithm ($G_{\rm dB}$), gain in linearity ($G_{\rm Lin}$), average noise temperature (T_e), noise contribution to system ($\triangle T$) and output 1 dB compression point ($P_{\rm out-1\,dB}$) of each microwave part in receiver chain are shown in Table 2. Wherein, the calculated system specifications are as follows: gain is 83.33 dB; output 1 dB compression point is 10 dBm; receiver noise is 13.64 K as referred to the input of the cryogenic Dewar, and 33.76 K as referred to the feed aperture plane.

2.1. Ultra-wide Bandwidth Feed

The proposed UWB feed is based on circular QRFH body with a concentric-loaded dual-layer dielectric spear, and non-differential dual-linearity polarizations are adopted. Four ridges with optimal exponential curve profile are inserted in the flared hollow horn to enlarge the relative bandwidth: the edge capacitance effect of the inserted ridges increases the cutoff wavelength of the dominant mode of TE_{11} in the circular waveguide and decreases the cutoff wavelength of the next higher order mode. Theoretically, exponential curves, conic

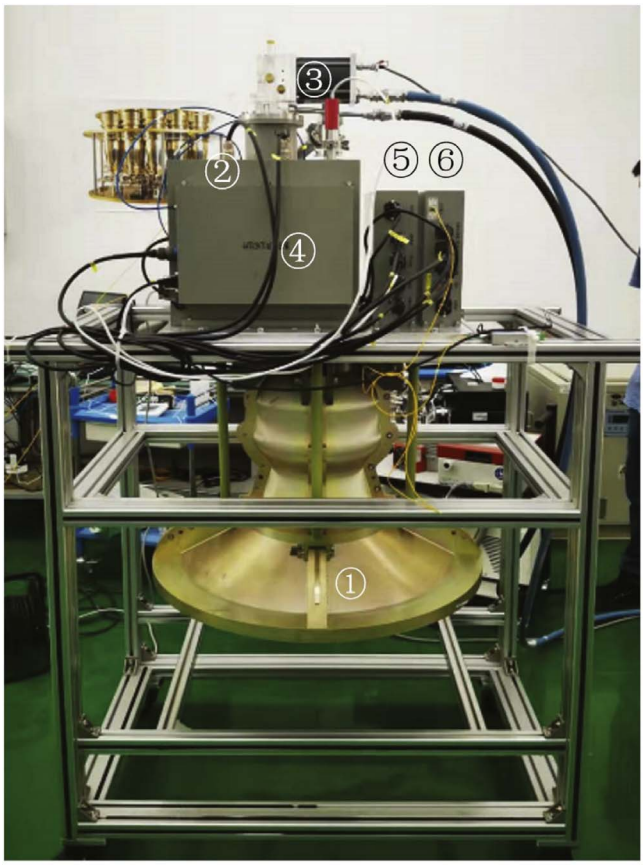

Figure 2. Photographs of assembled 0.5–3.3 GHz cryogenic receiver. QRFH①, cryogenic Dewar②, cryocooler③, calibrating noise unit④, system power supply and monitoring unit⑤ and optical transmitter⑥ can be seen.

curves, and Gaussian curves can all be employed in ridges profiles. In order to improve the innovation design space and the overall performance, an amended exponential Equation (2) is used as ridges profile in the optimal simulation of the proposed QRFH

$$p(x) = \alpha e^{\beta x} + \gamma x + \delta. \quad (2)$$

Wherein, α and β are the adjustment factors related to the aperture of horn and the diameter of ridged waveguide. The first order item γx and the constant item δ are the amended items to the traditional exponential ridge curves. Teflon is used as the dual-layer dielectric spear material, and its profile fits the space shape held up by the ridge edges. The height and maximum diameter are 377 mm and 145 mm, respectively.

A 3D electromagnetic simulator CST Studio Suite (2016) is employed to implement feed optimal design. The primary optimization goal is to obtain high dish aperture efficiency and large ports return loss. The main optimization parameters are feed aperture, thickness and taper of ridges, width and depth of backshort, and gaps between opposite ridges. After multiple rounds of optimization, the optimal simulation model and the physical image of QRFH are shown in Figure 3.

2.2. Cryogenic Unit

A rectangular cryogenic Dewar is developed to provide vacuum and cryogenic environment to the directional couplers and LNAs. The structure sketch and physical image of Dewar are shown in Figures 4 and 5. Couplers and LNAs are thermally connected to the second stage (13 K) of cryocooler, and enclosed by a thermal radiation shield connecting to the first stage (42 K) of cryocooler. Low-loss thermal insulation cables are employed to interconnect the Dewar input ports and couplers, and its physical temperature gradually changes from 300 to 13 K with an average temperature of about 150 K and insertion loss of 0.15 dB.

The directional coupler is used to inject calibrating noise into the LNA. Because it is in front of LNA, the ohmic loss must be reduced by optimal design. A UWB ultra-low loss cryogenic directional coupler basing on strip line structure and two-layer circuits board is optimally designed and developed, and 0.107 dB of average insertion loss and 26 dB of average coupling coefficient are achieved, respectively. Advanced PTFE circuit substrate material Rogers RT5880 is adopted in view of its low loss (0.0009 in loss tangent) and cryogenic stability (12 ppm $^{\circ}C^{-1}$ in thermal change rate) features. Different with room temperature application, the microwave parameters of circuit board substrate in cryogenic temperature need to be accurately measured by fabricating resonant ring on the substrate under test. At 15 K physical temperature, the dielectric constant and loss tangent of RT5880 show good stability, which are 2.18 and 0.0008, respectively. The simulation model and physical image of the coupler are shown in Figure 6.

In view of better return loss and good overall performance, the cryogenic LNA of CITLF3 from CMT is selected as the first stage amplifier of the proposed receiver. CITLF3 is developed based on silicon-germanium (SiGe) HBT transistors, and its physical image is shown in Figure 7 (CITLF3 datasheet 2022). From 0.5 to 3.3 GHz: its input return loss is larger than 10 dB, which is crucial to achieve good power matching and then to prevent the occurrence of standing waves; the average noise temperature is 4.4 K at 12 K physical temperature, which helps to achieve good receiver noise as well as other low loss components in front of it; the average power gain is about 34 dB at 12 K, it is high enough for suppressing the noise contribution of post-stage components of receiver according to Equation (1).

In order to divide the calibrating noise into the two polarization channels of receiver, a UWB cryogenic power splitter is developed based on Wilkinson strip line structure (Tseng & Wu 2010). The parameters measurement method of circuit board substrate at cryogenic temperature is the same as coupler, and the physical image of splitter is shown in Figure 8.

Table 2
Main Specifications Breakdown of Receiver Microwave Chain

Microwave Parts	T_{amb} (K)	G_{dB} (dB)	G_{Lin}	T_e (K)	$\triangle T$ (K)	$P_{out-1\ dB}$ (dBm)
Feed	300	−0.15	0.966	10.54	10.54	
Warm cable	300	−0.12	0.973	8.40	8.70	
Hermetic connector	300	−0.03	0.993	2.08	2.21	
Insulation cable	150	−0.15	0.966	5.27	5.65	
Cryogenic coupler	15	−0.12	0.973	0.42	0.47	
Cryogenic cable	15	−0.20	0.955	0.71	0.81	
Cryogenic LNA	15	34.00	2511.886	4.40	5.25	0
Insulation cable	150	−0.40	0.912	14.47	0.00	
Warm cable	300	−0.50	0.891	36.61	0.02	
Post amplifier 1	300	36.00	3981.072	150	0.09	5
Optical transceiver	300	−20.00	0.010	91416	0.01	10
Splitters network	300	−7.00	0.199	1203	0.00	
Mixing unit	300	42.00	15848.931	600	0.00	15
System specs		83.33			33.76	10

From 0.5 to 3.3 GHz and at 15 K physical temperature, 3.08 dB of total loss, ohmic loss lower than 0.1 dB and isolation larger than 20 dB are achieved

$$T_{leak} = \frac{1}{L_{co}}\left(T_{sp} + \frac{T_{ns}}{L_{nc}}\right). \quad (3)$$

The total leaking noise T_{leak} of coupling link from noise source unit at constant temperature of 308 K to cryogenic LNA can be figured out from Equation (3), wherein, L_{co} is the coupling attenuation of cryogenic coupler (26 dB); T_{sp} and L_{nc} is the physical temperature (12 K) of the splitter (including the interconnecting cables) and total attenuation (5.2 dB) of the splitter, the interconnecting cables and the hermitic connector; T_{ns} is the physical temperature of noise source unit box (308 K). So the calculated leaking noise is only about 0.26 K as noise source is switched off.

2.3. Warm Electronics and Electro-optical Units

From the receiver block diagram in Figure 1, post amplifier 1 with a gain of 36 dB is inserted between the Dewar and the optical transceiver. The gain of second stage amplifier higher than 30 dB is necessary to suppress the noise contribution of the very noisy optical transceiver behind it, especially for the receiver system with uncooled feed like this paper. From Table 2, it can be seen that the noise contribution arising from optical transceiver to receiver system is only 0.01 K.

The 0.5–3.3 GHz UWB optical transceiver is developed to implement full bandwidth microwave signals transmission over about 3 km long high stability optical fiber (Liu et al. 2017) from the receiver cabin to the digital backend on the ground. The UWB optical transceiver is fabricated based on Distributed Feedback laser with 1310 nm wavelength and optical detector with non-sensitive feature to laser polarization: the optical wavelength of 1310 nm is better in low dispersion transmission; non-polarization sensitive detector helps to improve the power stability of transmission. The mechanism of "electro-optical-electro" conversion can be described by Equation (4)

$$i_o = \frac{\eta I_i \pi V_m}{2 v_\pi}. \quad (4)$$

Wherein, i_o is the output photocurrent; η is the sensitivity of optical detector; I_i is the incident optical power; V_m is the voltage of input microwave signal; V_π is half-wave voltage of optical modulation. The noise temperature of optical transceiver is about 91,000 K, and the gain of optical link is −20 dB. The full bandwidth optical transmission is helpful to improve the power and phase consistency of sub bands and simplify the complexity of receiver in receiver cabin. The physical image of optical transceiver is shown in Figure 9.

2.4. Warm Filtering and Mixing Units

The 0.5–3.3 GHz output signals of optical receiver are split and filtered to form four sub frequency bands by the filters

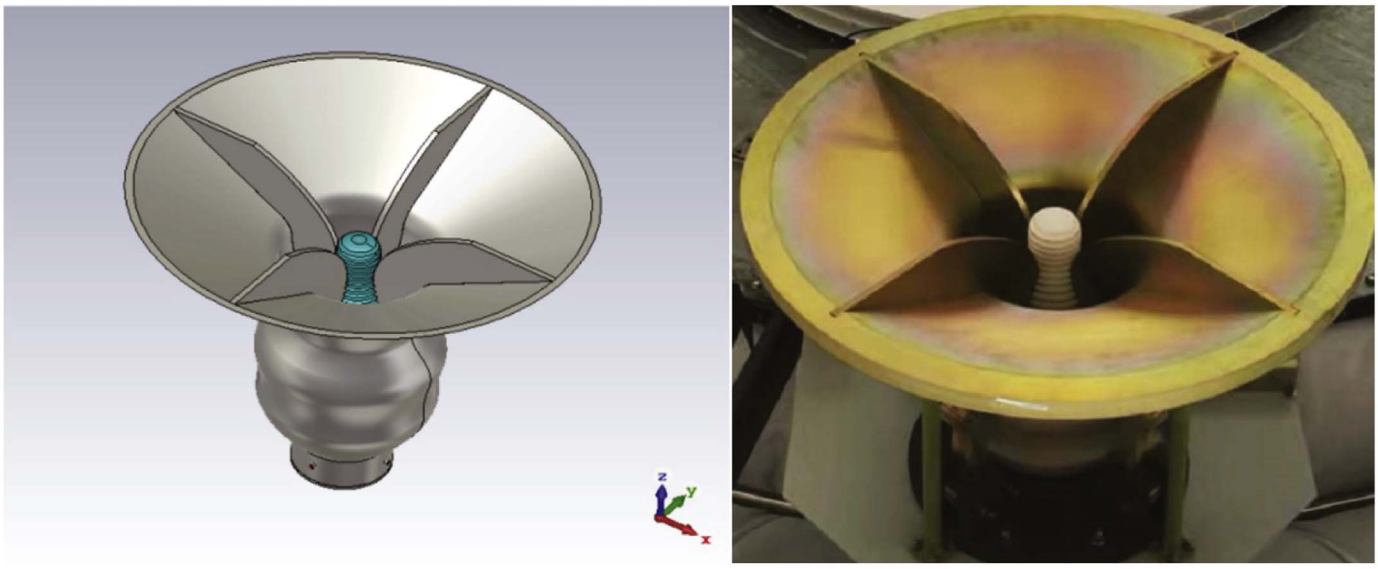

Figure 3. Simulation model (left) and photograph (right) of Quad-Ridged Flared Horn. Horn body, four ridges and concentric-loaded dual-layer dielectric spear can be seen. The aperture, diameter at feet point and height of horn are 860 mm, 300 mm and 667 mm, respectively.

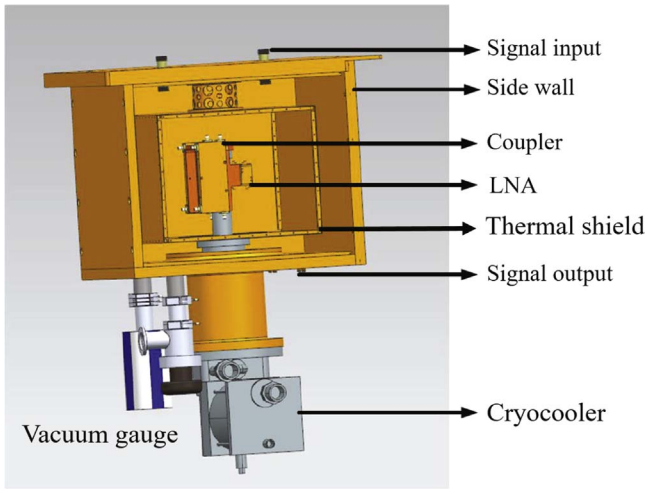

Figure 4. Structure sketch of cryogenic Dewar with front panel removed.

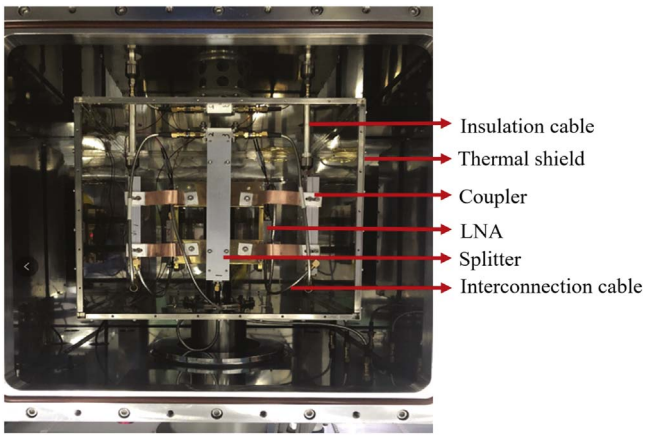

Figure 5. Photograph of cryogenic Dewar with front panel removed.

and splitters network seen in Figure 1: 0.5–1 GHz ;(subCH1), 0.9–1.8 GHz (subCH2), 1.7–2.6 GHz (subCH3) and 2.5–3.3 GHz (subCH4). By amplifying and further filtering, the signals of SubCH1 are directly sampled by digital backend, while, the signals of subCH2, subCH3 subCH4 need to be down converted to 0.1–1 GHz before digital backend. The gain of post amplifier 2 is about 35 dB; in order to prevent sampling aliasing in digital backend, bandpass filters with high stopband rejection performance is fabricated. The last stage bandpass filters in each subchannel are designed to have a stopband rejection higher than 40 dB at 1.2 GHz; the 1.9 GHz, 2.7 GHz and 3.5 GHz high local oscillating (LO) mixing signals are used to down-conversion of subCH2, subCH3 and subCH4 respectively, and the average conversion loss of mixers are 9 dB; digital attenuators with intrinsic loss of 1.5 dB can provide a gain adjustment range of 30 dB with the steps of 1, 5 and 10 dB to cope with different interference signal powers; the IF amplifier 1 (15 dB gain) and amplifier 2 (15 dB gain) are used to provide appropriate signal power (about −15 dBm of sub bandwidth power) to the linearity range of digital backend (255 digital values for 8-bit sampling).

3. Modules and System Measurement

3.1. Quad-ridged Flared Horn

The radiation patterns of QRFH were measured in a microwave anechoic room (shown in Figure 10) by Agilent E5071C Vector Network Analyzer (VNA). The measured and

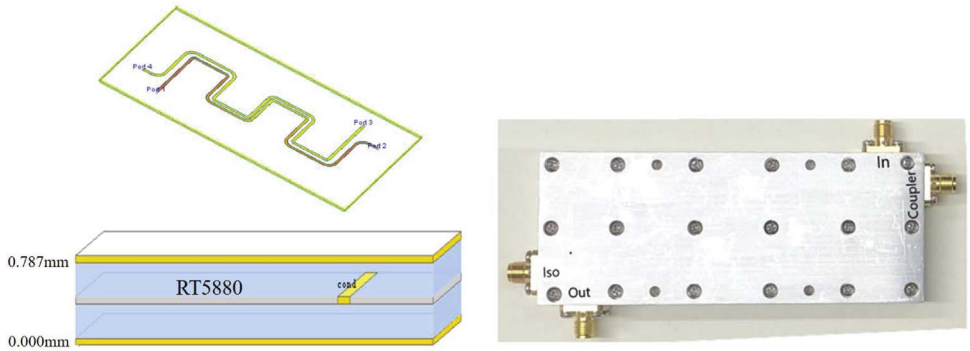

Figure 6. Simulation model (left) and photograph of cryogenic coupler. Strip line structure (top) and circuit board with dielectric substrate (bottom) can be seen.

Figure 7. Photograph of CITLF3. The bias situation in this application are: 2 V of V_{ds} and 13.6 mA of I_{ds}.

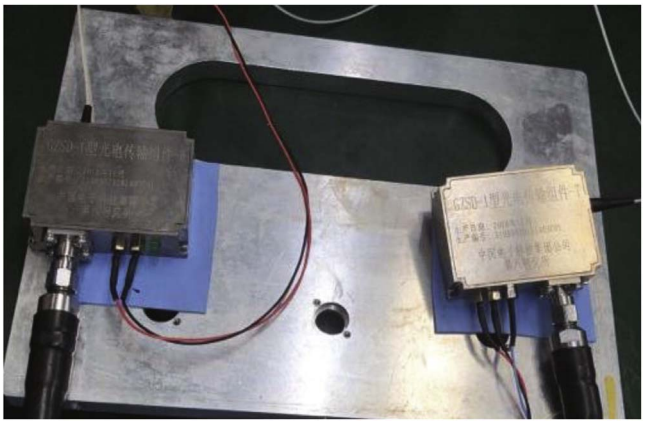

Figure 9. Photograph of optical transceiver.

Figure 8. Photograph of cryogenic splitter.

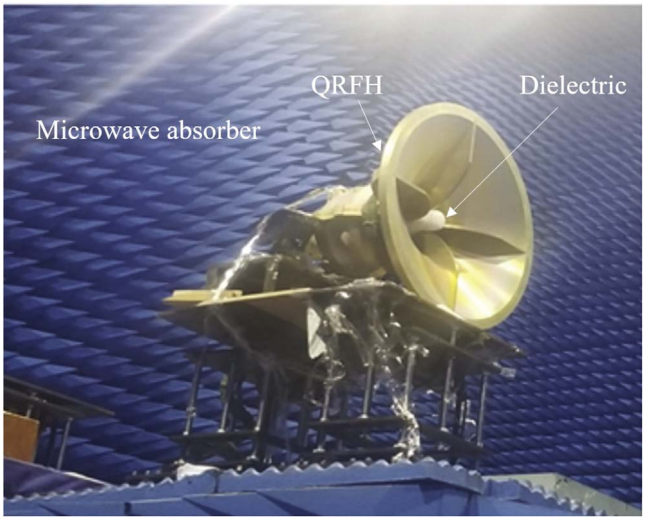

Figure 10. Radiation pattern measurement setup of QRFH in 10 m microwave anechoic room.

simulated *E*-plane and *H*-plane, and the simulated *D*-plane co and cross polarization radiation patterns are shown in Figure 11. It can be seen that the measured results fit well with the simulated results no matter *E*-plane or *H*-plane in the full working bandwidth, especially for the band of 0.5–3 GHz. In addition, the simulated and measured axial cross-polarization level of the QRFH are shown in Figure 12. For the ideal rotationally symmetric simulation model of circular horn, the simulated cross-polarization levels are always very low (lower than -65 dB), and the machining deviation between the assembled horn and its model worsens the cross polarization level, but the cross polarization level on the passband is still less than -30 dB. The simulated phase center positions varying with frequencies are shown in Figure 13 and the maximum deviation is $0.316\lambda_c$ (λ_c: central wavelength) over the ultra-wide working bandwidth of 2.8 GHz. The simulation of dish aperture efficiency and dish gain with physical optics method are implemented in an antenna simulator (TICRA Grasp 2022)

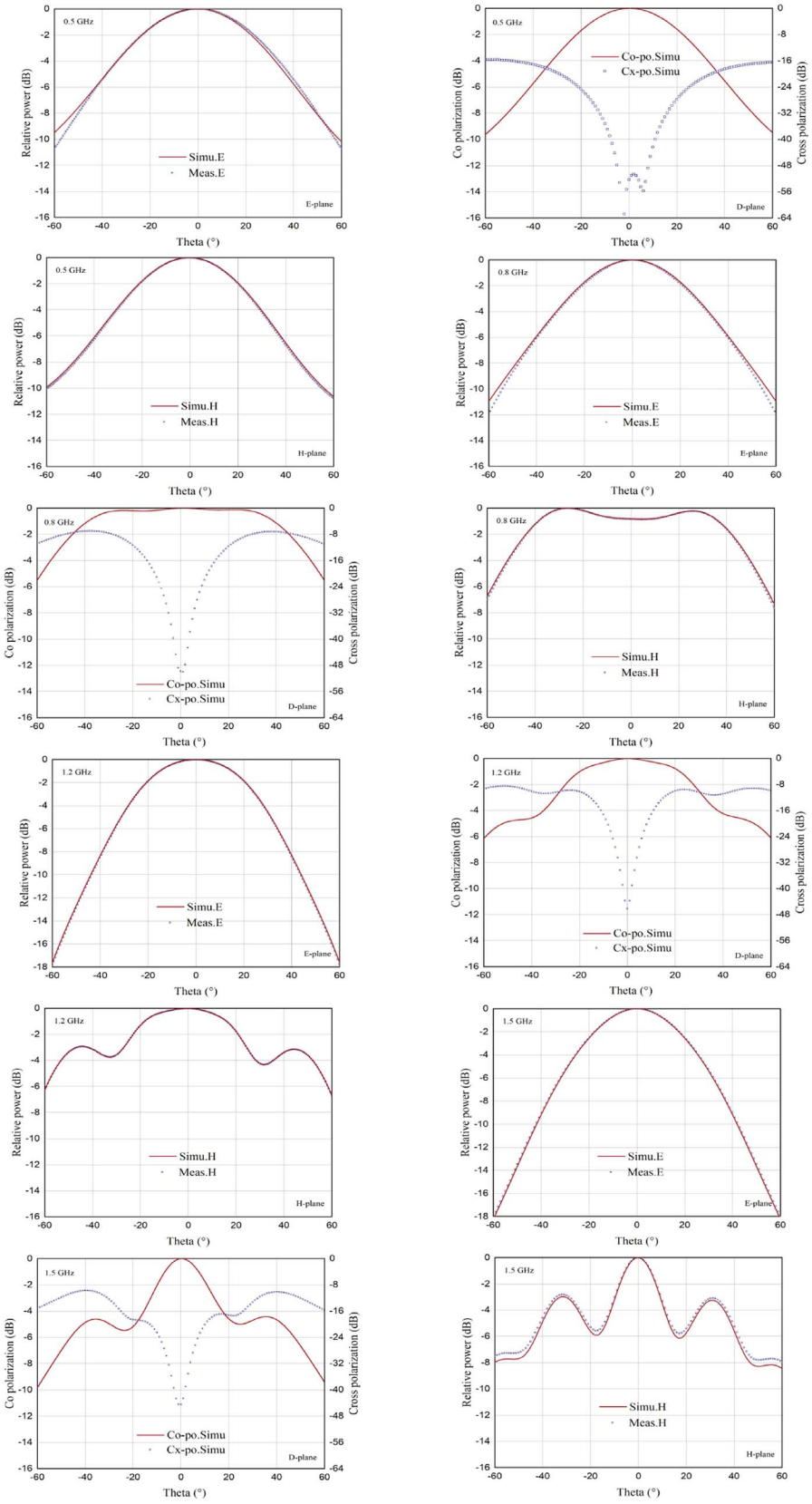

Figure 11. Measured and simulated *E*-plane and *H*-plane, and simulated *D*-plane co polar and cross polar normalized radiation patterns of QRFH at 0.5, 0.8, 1.2, 1.5, 2.3, 2.7, 3.0 and 3.3 GHz.

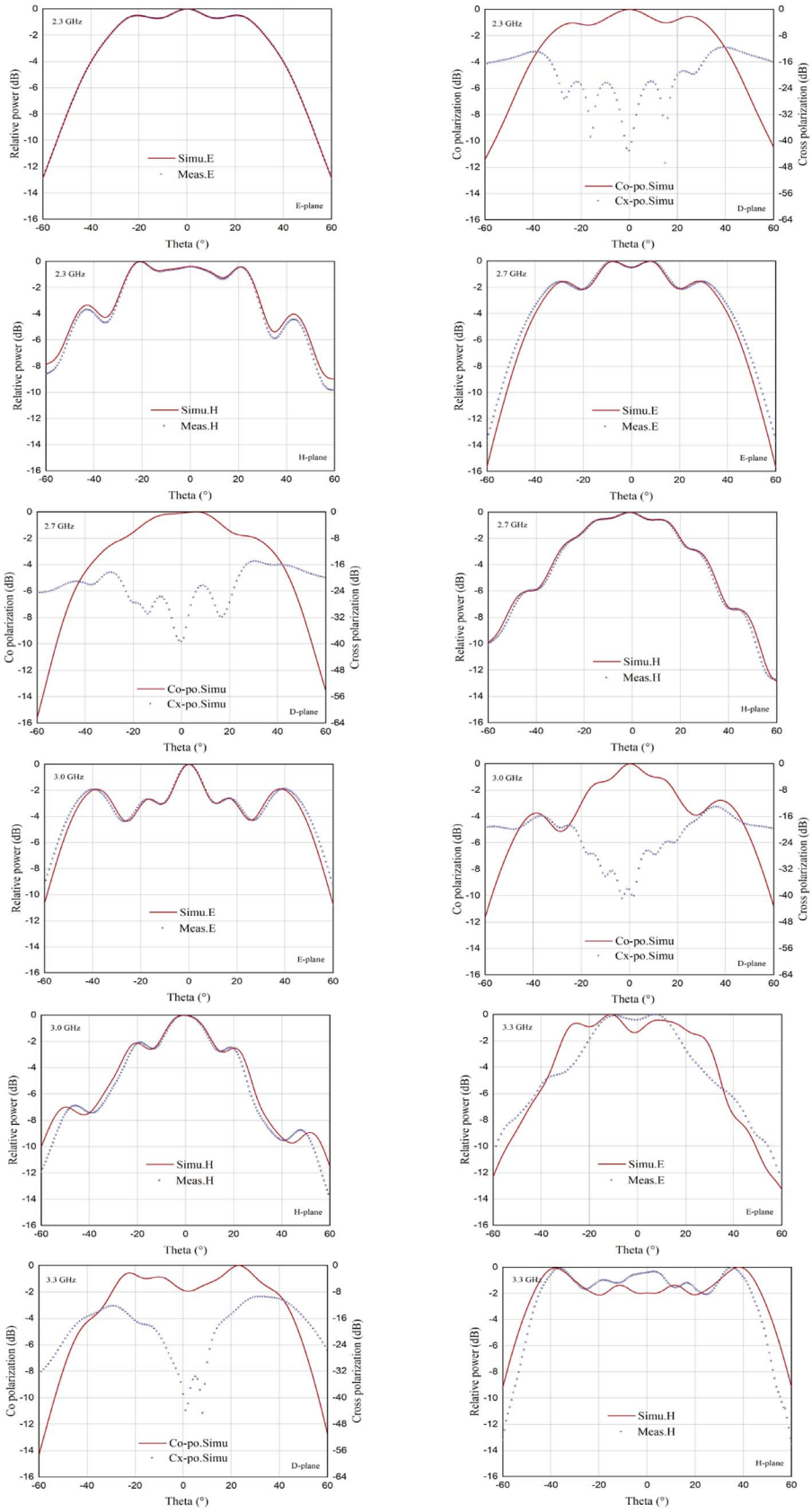

Figure 11. (Continued.)

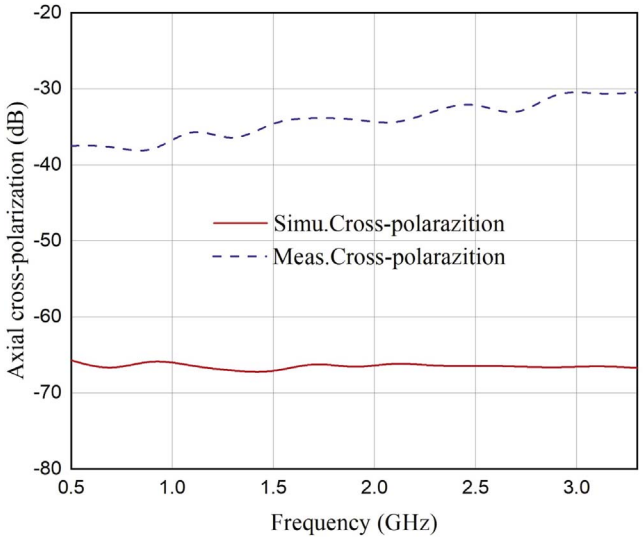

Figure 12. Simulated and measured axial cross-polarization levels of QRFH.

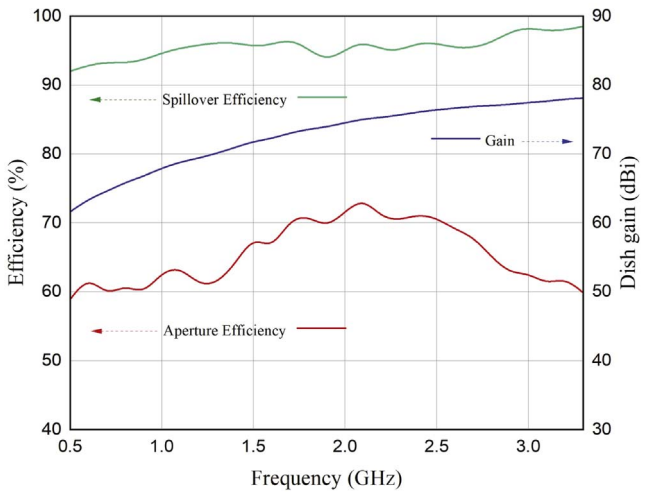

Figure 14. Simulated dish aperture efficiency, spillover efficiency and dish gain.

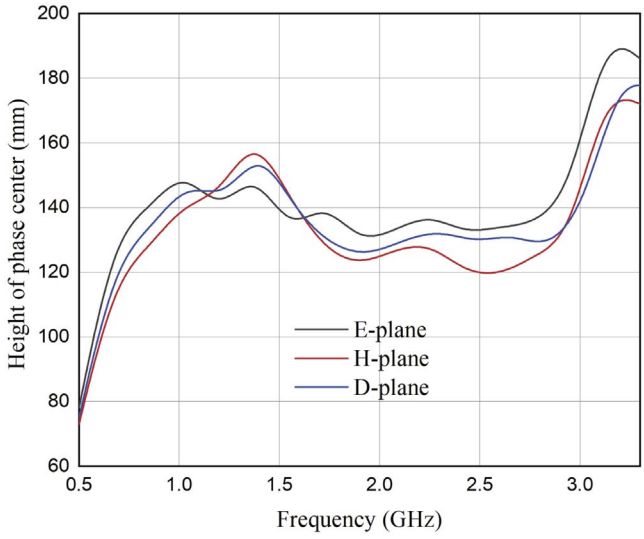

Figure 13. Simulated height of *E*-plane, *H*-plane and *D*-plane phase center to aperture plane of QRFH within the subtended angle of 112°.8.

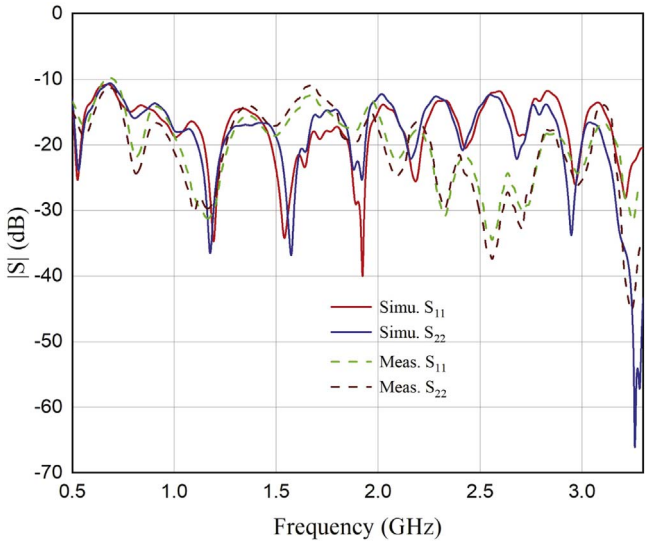

Figure 15. Measured and simulated S_{11} and S_{22} of QRFH.

based on the measured horns radiation pattern and continuous FAST reflector model. Dish aperture efficiency higher than 60% (65.7% in average) and dish gain larger than 60 dBi (72.6 dBi in average) were achieved (see Figure 14). Holes on the reflector panels, gaps between the reflectors and dish shape deviations from the ideal paraboloid will lower the real dish efficiency and gain, and the actual test for dish efficiency and gain will be implemented before the astronomy observation with the proposed UWB receiver.

The Scattering parameters (S-parameters) of QRFH were measured with horn facing to the sky by using VNA. The return loss of two ports, and ports polarization isolation can be figured out by this measurement. The measured results of S_{11} and S_{22} as well as the corresponding simulated results are shown in Figure 15. Figure 15 shows that the reflection coefficient of two ports are all lower than -10 dB, and the average reflection coefficient of H and V polarization is -20.21 dB and -21.26 dB, respectively. The measured ports polarization isolation as well as the simulated curves are shown in Figure 16. The simulated and measured results meet well within the full band, and the isolation is greater than 40 dB up to 2.7 GHz and greater than 38 dB under 3.3 GHz. The average isolation is 43.87 dB, which can evidently eliminate crosstalk between two channels of the receiver.

Compared with other main low-frequency QRFH for prime focus illumination worldwide (shown in Table 3), the above

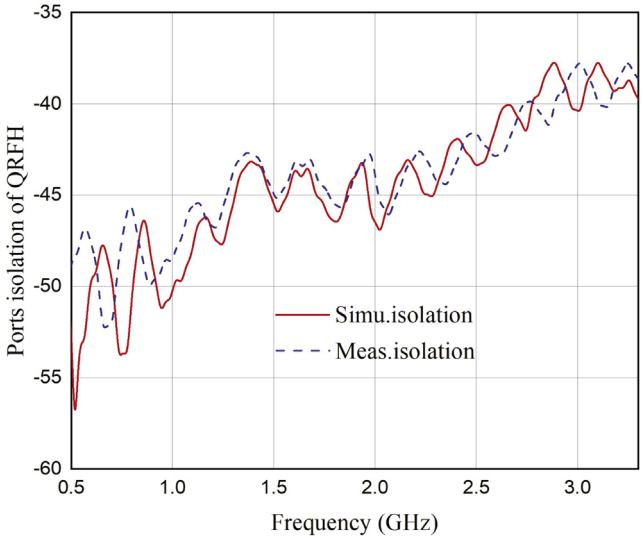

Figure 16. Measured and simulated results of ports polarization isolation of QRFH.

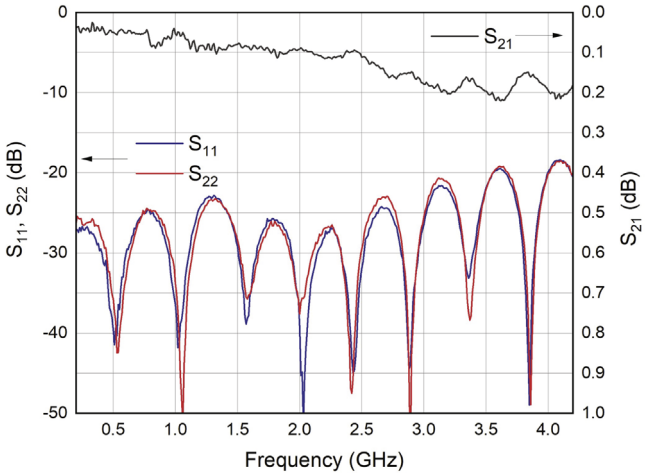

Figure 17. Measured main channel S-parameters of Coupler at 15 K. Subscripts 1 and 2 in S-parameters note the "In" and "Out" ports of Figure 6, respectively.

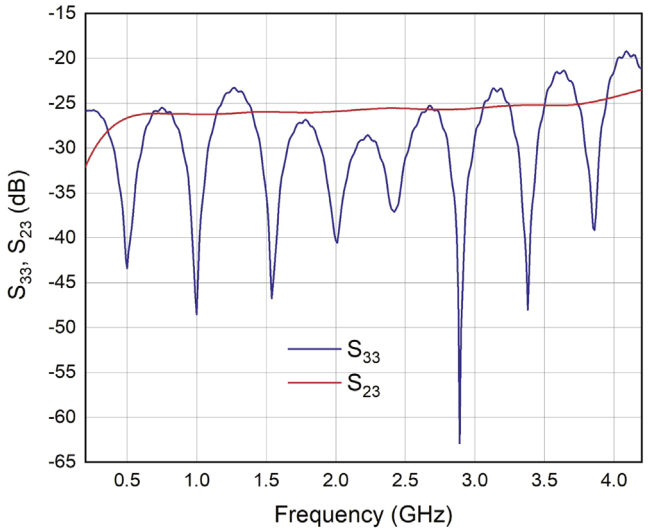

Figure 18. Measured coupling channel S-parameters of Coupler at 15 K. Subscript 3 in S-parameters notes the "coupling" port of Figure 6.

results show good performances of the proposed QRFH in wider relative bandwidth.

3.2. Cryogenic Components

The S-parameters of the directional coupler of the proposed receiver are measured at the physical temperature of 15 K by Keysight N5232B 4-port VNA and cryogenic testing Dewar. The measurement results of main channel are shown in Figure 17. It shows that the coupler has excellent loss and good reflection characteristics: the mainline loss (S_{21}) is lower than 0.2 dB and the average loss is only 0.107 dB from 0.5 to 3.3 GHz. This means that the coupler at 15 K physical temperature exports only 0.37 K noise to the system links; the reflection coefficients of the input and output ports of the main channel are lower than −20 dB over the passband, which helps to achieve good power matching with the feed and LNA. The measured S-parameters of coupling channel are shown in Figure 18. It shows that the coupling attenuation ($|S_{23}|$) is larger than 25 dB (average in passband: 25.9 dB) and the reflection coefficient of coupling port (S_{33}) is far lower than −20 dB from 0.5 to 3.3 GHz. The coupling attenuation of about 26 dB is an appropriate value to suppress the leaking noise of noise injection unit (seen in Equation (3)) and provide reasonable calibrating noise power (10 and 1 K levels) generating from available UWB solid-state noise source with the limited ENR (NC3101 datasheet 2022).

The S-parameters of the power splitter of the proposed receiver are measured at the physical temperature of 15 K by Agilent N5232B VNA and cryogenic testing Dewar. The measurement results are shown in Figure 19. It shows that the return loss of the input and "out1" ports is larger than 20 dB and 18 dB from 0.5 GHz to 3.3 GHz, respectively. The average insertion loss above 3 dB is 0.079 dB, which corresponds to the ohmic loss from the input port to one of the output branch.

The noise temperature of cryogenic LNAs applied in the receiver at the physical temperature of 15 K were measured by a cryogenic noise testing system based on Variable Load Temperature method (Zhang et al. 2010). The measured results are shown in Figure 20. The average noise temperature of *H* and *V* polarization are 4.45 and 4.33 K from 0.5 to 3.3 GHz.

3.3. Receiver System

The Keysight N9010B signal analyzer is used to measure the amplitude–frequency response of the proposed receiver. The

Table 3
Comparison of Key Specifications of Main Low-frequency Prime Focus QRFH Worldwide

Development Institutions	Operating Frequencies	Relative Bandwidth	Subtended Angle	Return Loss	Average Aperture Efficiency
PRETORIA UNIV (Jacobs et al. 2013)	0.75–3 GHz	4:1	70°	>13 dB	60%
CALTECH (Akgiray et al. 2013)	2–12 GHz	6:1	85°	>10 dB	58%
CSIRO (Dunning et al. 2015)	0.7–4.2 GHz	6:1	96°	>14 dB	65%
STELLENBOSCH UNIV(Beukman 2015)	2–12 GHz	6:1	86°	>15 dB	55%
CALTECH (Smith & Weinreb 2016)	0.27–1.62 GHz	6:1	110°	>10 dB	60%
This paper	0.5–3.3 GHz	**6.6**:**1**	110°	>10 dB	**65**%

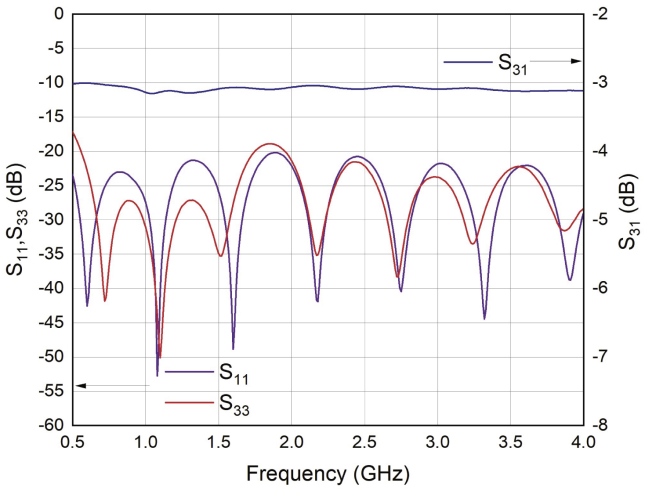

Figure 19. Measured S-parameters of power splitter at 15 K. Subscripts 1 and 3 in S parameters notes "In" and "Out1" ports of Figure 8.

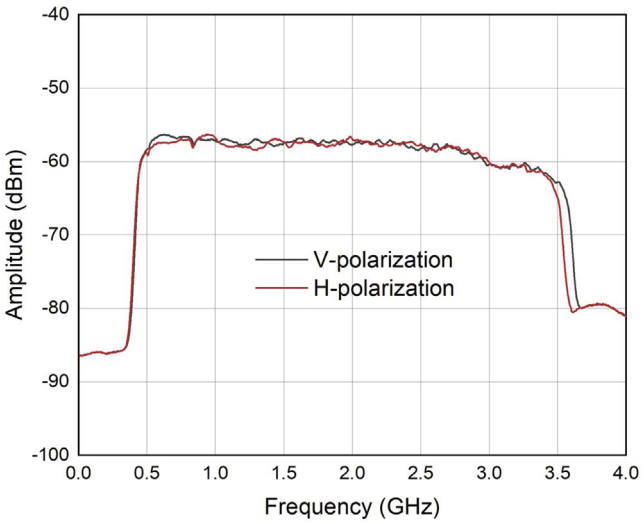

Figure 21. Measured full band amplitude–frequency response of two polarization channels of UWB receiver. The measurement reference plane is the output of optical transceiver shown in Figure 1. The input ports of Dewar are terminated by 50 Ω loads.

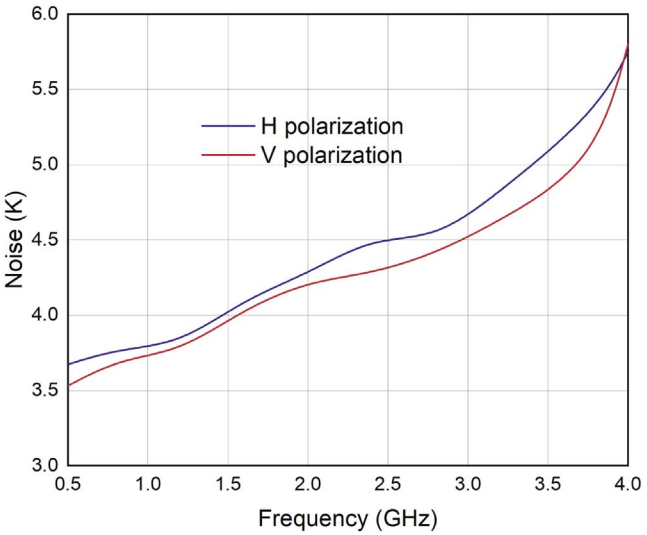

Figure 20. Measured noise temperature of cryogenic LNAs in the *H* and *V* polarization of receiver. The test is under the bias of 2 V and 13 mA.

measured full band response is shown in Figure 21. It shows good passband flatness. The flatness is better than ±1.18 dB from 0.5 to 2.8 GHz and better than ±2.2 dB over the full working bandwidth of 0.5–3.3 GHz. In addition, the passband consistency between *H* and *V* polarization is very good. The measured sub channels response of *H* polarization are shown in Figure 22. Wherein, the displaying frequencies of subCH1 is forward, and those in the other three sub channels are reverse because of the frequency conversion by mixers. The sub channels response of *V* polarization is basically the same with *H* polarization.

Digital attenuators can provide 30 dB gain adjustment range with the steps of 1, 5 and 10 dB. The measured response with six gain levels of subCH3 *H* polarization is shown in Figure 23. The function of gain adjustment helps to set appropriate power levels of receiver according to various astronomy sources and RFI situations.

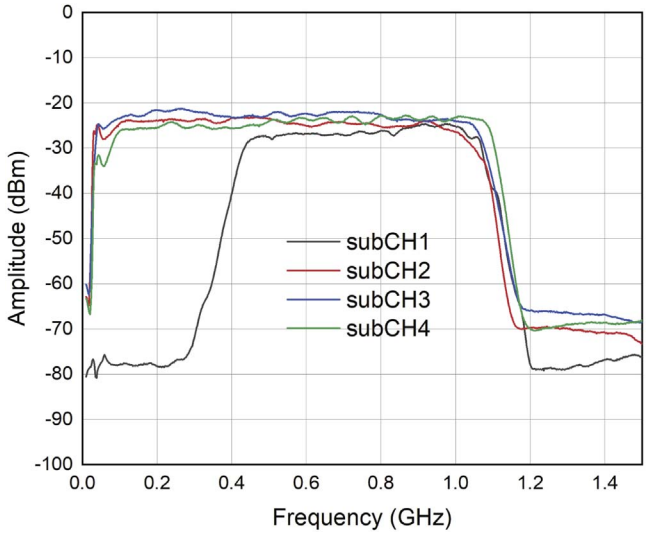

Figure 22. Measured amplitude–frequency response of four sub channels of the *H*-polarization channel of the UWB receiver. The measurement reference plane is the IF output P1 of UWB receiver shown in Figure 1. The input ports of Dewar are terminated by 50 Ω loads.

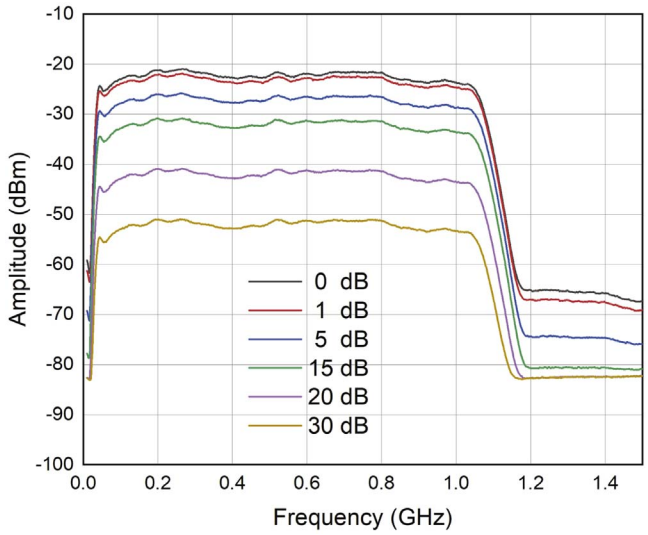

Figure 23. Measured amplitude–frequency response of subCH3 in the *H*-polarization channel of the UWB receiver under six different gain levels.

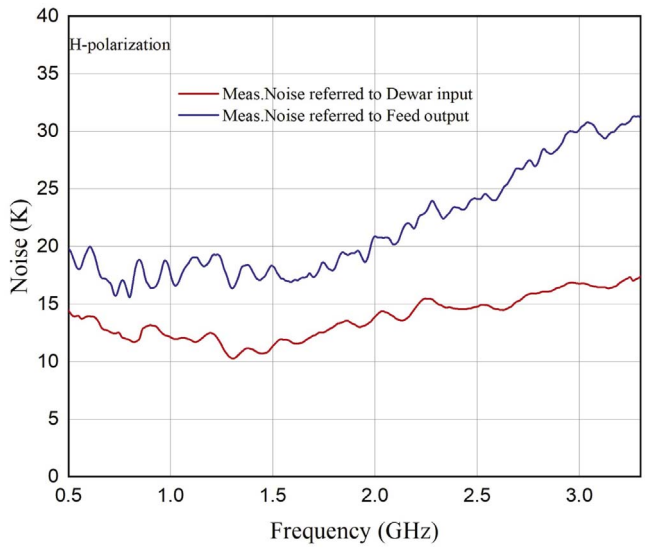

Figure 24. Measured noise temperatures of *H* polarization channel. Moving average with 10 adjacent frequency points for the measured data was implemented to achieve average noise level hiding in the time invariant interference.

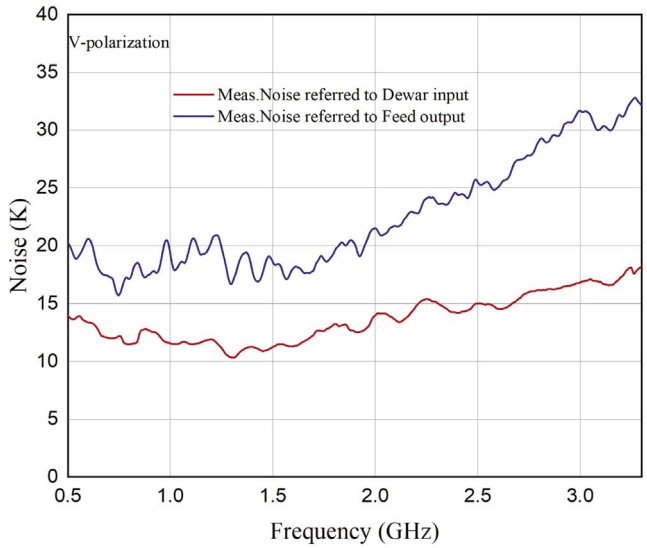

Figure 25. Measured noise temperatures of *V* polarization channel. Moving average with 10 adjacent frequency points for the measured data was implemented to achieve average noise level hiding in the time invariant interference.

The Keysight N8975B noise figure analyzer is used to measure the noise temperature of the cryogenic receiver. The measured noise temperatures of *H*-polarization of the receiver are shown in Figures 24 and 25. 10 times trace average for the measured noise is set in noise figure analyzer to eliminate time-varying interference. The *H*-polarization average noise temperatures referred to the input of Dewar and the output of feed in the passband are 13.79 K and 21.71 K, respectively. Those for *V*-polarization are 14.15 K and 22.49 K, respectively. The analysis of QRFH noise temperature is implemented by simulating the ohmic loss of QRFH. The ohmic loss from the coaxial port to the aperture of QRFH is figured out by energy radiation efficiency simulation of 3D electromagnetic simulator CST Studio Suite (2016). The simulation results are shown in Figure 26, which shows that the average ohmic loss of feed as a whole, the metal of feed and the dielectric of feed are 0.1511 dB, 0.0858 dB and 0.0653 dB, respectively. To ensure the consistency of the simulation loss with the real loss, the internal surface roughness of Ra 1.6 (1.6 μm) of feed aluminum

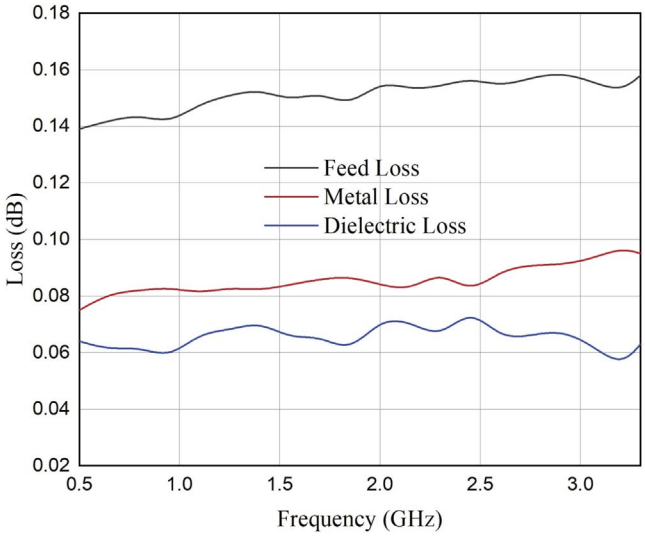

Figure 26. Simulated ohmic loss of feed as a whole, the metal of feed and the dielectric of feed. Internal surface roughness of Ra 1.6 (1.6 μm) of feed aluminum material and dielectric loss tangent of 0.0003 of high-purity teflon inside feed are set in simulation model.

material required in manufacturing and the dielectric loss tangent of 0.0003 of high-purity teflon applied in the actual feed are set in the simulation model. The feed loss of 0.15 dB means that the noise temperature of QRFH at 300 K is 10.54 K (listed in Table 2), therefore, the total noise of the receiver system is at the level of about 33 K. The actual test of the noise temperature of the receiver with QRFH will be implemented when the 19-beam receiver is replaced by the proposed cryogenic UWB receiver in the future.

4. Summary

We have developed a low-frequency UWB cryogenic receiver for FAST telescope and described its main performance. This receiver covers the frequency band from 0.5 to 3.3 GHz and expands the bandwidth of the low-frequency UWB receiver to 6.6:1. Compared with the first UWB cryogenic receiver of FAST, the proposed receiver has wider relative and absolute bandwidths, and can cover over 95% working band of FAST telescope. It means that the specifications of S-parameters, noise temperature, gain and gain flatness of all microwave and optical parts need to be good in wider band. It will improve the capability of multi-spectrum lines detecting and real-time UWB observatories of FAST telescope. Several key UWB and low-loss microwave components were developed to meet the requirements of the proposed receiver. These components as well as the corresponding technologies are helpful for further development of receivers.

Acknowledgments

This work was supported by the National Key R&D Program of China (2018YFE0202900) and the National Natural Science Foundation of China (U1831110).

References

Akgiray, A., Weinreb, S., Imbriale, W. A., et al. 2013, ITAP, 61, 1099
Bardin, J. C., & Weinreb, S. 2010, in Proc. 5th European Microwave Integrated Circuits Conf. (*Paris, France, 27–28 September*) (EuMA), 186
Beukman, T. S. 2015, PhD dissertation, Dep. Electrical and Electronic Engineering Stellenbosch Univ, Stellenbosch, South Africa
CITLF3 datasheet 2022, https://www.cosmicmicrowavetechnology.com/citlf3
CST Studio Suite 2016, Computer Simulation Technology Corporation, Darmstadt, Germany, https://www.3ds.com/products-services/simulia/products/cst-studio-suite
Dunning, A., Bowen, M., Bourne, M., et al. 2015, in Antennas and Propagation in Wireless Communications (APWC), 2015 IEEE-APS Topical Conf. (*Torino, Italy, 7–9 September*)(IEEE), 787
Hobbs, G., Manchester, R. N., Dunning, A., et al. 2020, PASA, 37, 1
Hopfer, S. 1955, IRE Trans. Microw. Theory Tech., 3, 20
Jacobs, O. B., Odendaal, J. W., & Joubert, J. 2013, ITAP, 61, 2948
Jiang, P., Tang, N.-Y., Hou, L.-G., et al. 2020, RAA, 20, 064
Liu, H., Pan, G., Lin, Z., et al. 2017, OptFT, 38, 1
LNC0.3-14A datasheet 2022, https://lownoisefactory.com
Nan, R. 2006, ScChG, 49, 129
NC3101 datasheet 2022, https://noisecom.com/Portals/0/Datasheets/nc3000-coaxial-noise-sources-datasheet.pdf
Qian, L., Pan, Z., Li, D., et al. 2019, ScChG, 62, 959508
Smith, S., & Weinreb, S. 2016, in Progress in Electromagnetic Research Symp. (PIERS), (*Shanghai, China 8–11 August*), (IEEE), 1666
Sun, W., & Balanis, C. A. 1994, ITMTT, 42, 2201
Thirumaleshwar, M., & Subramanyam, S. V. 1986, Cryo, 26, 547
TICRA Grasp 2022, TICRA Corporation, Copenhagen, Denmark, https://www.ticra.com
Tseng, C.-H., & Wu, C.-H. 2010, ElL, 46, 1327
Weinreb, S., Bardin, J. C., & Mani, H. 2007, ITMTT, 55, 2306
Yang, J., Pantaleev, M., Kildal, P.-S., et al. 2011, ITAP, 59, 1918
Zhang, S. G., Li, B., Zhu, X. Q., et al. 2010, J. Cryogenics and Superconductivity, 38, 76